Environmental Science
Water Research & Technology

ROYAL SOCIETY OF CHEMISTRY

PAPER

View Article Online
View Journal | View Issue

Cite this: *Environ. Sci.: Water Res. Technol.*, 2020, **6**, 935

Emerging investigator series: control of membrane fouling by dissolved algal organic matter using pre-oxidation with coagulation as seawater pretreatment†

Bhaskar Jyoti Deka, [a] Jiaxin Guo,[a] Sanghyun Jeong,*[b] Manish Kumar [c] and Alicia Kyoungjin An *[a]

Received 26th October 2019,
Accepted 25th January 2020

DOI: 10.1039/c9ew00955h

rsc.li/es-water

Marine algae produce organic matter, namely algal organic matter (AOM), especially during a harmful algal bloom. AOM has been recognised as a key cause for the formation of organic fouling on membranes in seawater desalination applications. In this study, pre-oxidation of AOM by potassium permanganate ($KMnO_4$) and sodium hypochlorite (NaOCl) was investigated. In addition, ferric (Fe^{3+}) and alum (Al^{3+}) coagulants were used for subsequent coagulation. Two different operational modes, conventional coagulation–flocculation–sedimentation (CFS) and coagulation–flocculation-dissolved air flotation (CF-DAF) processes, were used to evaluate pretreatment performance using synthetic AOM with an initial dissolved organic carbon (DOC) of around 4.8 mg C L^{-1} (turbidity ≈ 4.47 NTU, pH ≈ 8). Pre-oxidation with coagulation removed more AOM, compared to oxidation or coagulation alone. The removal of DOC by NaOCl–Fe^{3+} is relatively high when compared to other combinations of oxidant and coagulant because of *in situ* ferrate (Fe^{6+}) generation, which was detected by the ABTS (2,2′-azino-bis(3-ethylbenzothiazoline-6-sulfonic acid))-ultraviolet visible (UV-vis) method. Pre-oxidation with 1.5 mg L^{-1} NaOCl followed by coagulation with 2.5–3.0 mg L^{-1} Fe^{3+} achieved a maximum DOC removal of 65–76% during the CFS treatment; while, the DOC removal could further increase up to 83–85% by introducing CF-DAF. Particularly, the NaOCl–Fe^{3+} treatment generated 1.31 mg L^{-1} of *in situ* ferrate (Fe^{6+}). Finally, pre-oxidation and coagulation coupled with DAF successfully reduced fouling and lowered flux decline in a microfiltration (MF) membrane. Non-invasive optical coherence tomography (OCT) was performed to monitor the fouling development on the MF membrane before and after pretreatment.

Water impact

Natural or algal organic matters composed of humic substance, polysaccharide, protein *etc.* can significantly foul the membranes during the seawater desalination. Formation of harmful disinfection by-products during conventional oxidation process is also a concerning issue. Dissolved air flotation with *in situ* generated green chemical, ferrate showed a great ability to mitigate the membrane fouling as demonstrated by a non-destructive monitoring technique.

1. Introduction

Water stress has become a serious global issue due to the rapid increase in population, global warming, and climate change.[1–6] To address this issue, desalination of seawater *via* reverse osmosis (RO) has become a widely used approach,[7–9] however, fouling on RO membranes results in higher desalination cost.[10–17] Adoption of a low pressure microfiltration (MF) membrane unit prior to RO is a cost-effective method for removing materials that are responsible for scaling and fouling on RO membranes.[18,19] It has been observed that dissolved algal organic matter (AOM) and natural organic matter (NOM) consisting of humic substances (HS), biopolymers (BP), polysaccharides (PS), proteins, *etc.* in seawater play a dominant role in membrane fouling.[20–22] Moreover, AOM results in membrane pore blockage and perpetual flux decline.[23,24]

[a] *School of Energy and Environment, City University of Hong Kong, Tat Chee Avenue, Kowloon, Hong Kong. E-mail: alicia.kjan@cityu.edu.hk*
[b] *Environmental Engineering, Pusan National University, Busan 46241, Republic of Korea. E-mail: sh.jeong@pusan.ac.kr*
[c] *Department of Earth Sciences, Indian Institute of Technology Gandhinagar, Gujarat – 382355, India*

† Electronic supplementary information (ESI) available: Fig. S1 and S2; Table S1. See DOI: 10.1039/c9ew00955h

Generally, SWRO pretreatment systems include coagulation/flocculation/sedimentation (CFS), dissolved air flotation (DAF), granular media filtration (GMF) and low pressure membranes (MF/UF).[19,25] It has been reported that CFS, GMF, and DAF remove dissolved AOM/NOM in a poor manner.[26,27] In the case of membrane pretreatment, large molecular weight fractions of AOM are effectively rejected, however their precursors and low molecular weight fractions could be passed; thereby reaching the main process (*i.e.*, RO) and causing additional fouling on the RO membrane.[28] Therefore, an alternative or additional pretreatment step is necessary to improve the feed water quality, to ensure stable SWRO operation.

Recently, an oxidation or pre-oxidation step has been introduced as a membrane pretreatment process.[29] It has also been reported that ferrate (Fe^{6+}) is an efficient oxidative, disinfectant, coagulant, and odour remover.[30–32] The redox potential of Fe^{6+} is 2.2 V which is much higher than other commonly used oxidants, such as chlorine (1.358 V), hypochlorite (1.482 V), and ozone (2.076 V).[33–36] Further, the highly disinfectant nature of Fe^{6+} works well for inactivation of *E-coli*, as well as other waterborne species.[37] During the oxidation process, Fe^{6+} is reduced to a lower oxidation state, *i.e.* Fe^{3+} ion or $Fe(OH)_3$; in which it also acts as a coagulant.[38–40] Nevertheless, disinfection by-products that are produced when Fe^{6+} is used instead of chlorine,[31,32] as a result of the chemical reaction between chlorine and NOM/AOM, are much lower than those produced during traditional chlorinated disinfection.[41,42] Therefore, Fe^{6+} is considered to be a green chemical and treatment using Fe^{6+} has been termed as a green technology.[43] In spite of the numerous advantages of Fe^{6+} application in water and wastewater treatment industries, its use was not practically feasible due to its high cost and instability.[44] As a result, its use may be triggered if Fe^{6+} can be chemically generated during the course of treatment process (*i.e. in situ* generation).

In this study, we evaluated the benefits of *in situ* generated Fe^{6+} by comparison with other conventional oxidants, such as permanganate ($KMnO_4$) and sodium hypochlorite (NaOCl) along with commonly used alum-(Al^{3+}) and iron-(Fe^{3+}) based coagulants in both conventional CFS and CF-DAF. A MF membrane was applied as the final barrier for particles generated during the CF and fouling monitoring window. As far as we know, this is the first trial of the application of *in situ* Fe^{6+} in DAF with MF in SWRO pretreatment. Therefore, this study is ultimately aimed at elucidating the occurrence of fouling on MF membranes under different CF and CF-DAF conditions. Development of fouling over the membrane surface and inside the pores is generally being observed by a destructive method, in which membranes are collected from the separation assembly for investigation under microscopic scales. The destructive approach has limitations as the formation of the fouling layer is damaged during preparation for investigation. Although, variable composite fouling layers are formed over the time at various areas of the membrane, the samples used in the fouling autopsy are significantly smaller parts of the whole membrane. To monitor the fouling at a mesoscale (mm-scale) level, we adopted a powerful *in situ* and non-invasive optical coherence tomography (OCT) technique in which high axial and spatial resolutions were analysed using image processing algorithms.[45,46] OCT can monitor fouling development up to the millimetre range without disturbing the filtration setup or destroying the membrane morphology. 2D and 3D images with high micron level resolutions were acquired by scanning with a probe beam.[47] In addition, destructive membrane autopsies were performed using scanning electron microscope (SEM) to further understand membrane fouling.

2. Methods

2.1. Materials

Coagulant stock solutions were prepared by dissolving ferric chloride hexahydrate ($FeCl_3{\cdot}6H_2O$ (Fe^{3+}), 97%, Alfa Aesar) and alum ($KAl(SO_4)_2{\cdot}12H_2O$, Sigma) in deionised (DI) water until a final concentration of 1000 mg L^{-1} was reached for both Fe^{3+} and Al^{3+}. Sodium hypochlorite (NaOCl, at chemically pure grade, activated chlorine not less than 5.2%, UNI-Chem) and potassium permanganate ($KMnO_4$, Sigma) were used as oxidants and diluted with DI water to obtain a final stock concentration of 1000 mg L^{-1} for both NaOCl and $KMnO_4$, which was stored at 4 °C prior to use. Three different model AOM compounds were used, namely sodium alginate (SA) sodium salt (Sigma-Aldrich), humic acid (HA) sodium salt (Sigma-Aldrich), and bovine serum albumin (BSA, Sigma-Aldrich). The stock solutions (1000 mg-C per L) were prepared by dissolving SA, HA, and BSA in DI water, separately. The pH was adjusted by using 0.1 N hydrochloric acid (HCl, ACS reagent, 95.0–98.0%, Sigma-Aldrich) and 0.1 N sodium hydroxide (NaOH, 98% pure, anhydrous, Sigma-Aldrich). 2,2-Azino-bis(3-ethylbenzothiazoline-6-sulphonic acid, ABTS, MP Biomedicals) was used to measure the Fe^{6+} concentration using the ABTS UV-vis method.

2.2. Experimental procedure

Both CFS and CF-DAF experiments were carried out using a standard DAF Jar test apparatus (Platypus, Australia) at room temperature (25 ± 2 °C) using 2 L jars as shown in Fig. 1a. Sodium chloride (NaCl) from Sigma-Aldrich (ACS reagent, ≥99.0%) and calcium chloride ($CaCl_2$) from Acros-Organic (96%) were used to make synthetic saline water with AOM model compounds. This untreated AOM model solution served as the control. In this study, each oxidant was applied a fixed dosage of 1.5 mg L^{-1} as well as varying doses (0–3.0 mg L^{-1}) of the respective coagulants to get different ratios of the oxidants and coagulants.

The experiment was divided into three parts (Fig. 1): (i) optimization of the dissolved AOM removal under CFS and CF-DAF conditions with synthetic saline water prepared using NaCl (35.0 g L^{-1}) and $CaCl_2$ (1.2 g L^{-1}) in DI water at pH 8; (ii) assessment of AOM removal efficiency in real seawater collected from Pak Shek Kok Landing, Hong Kong Science

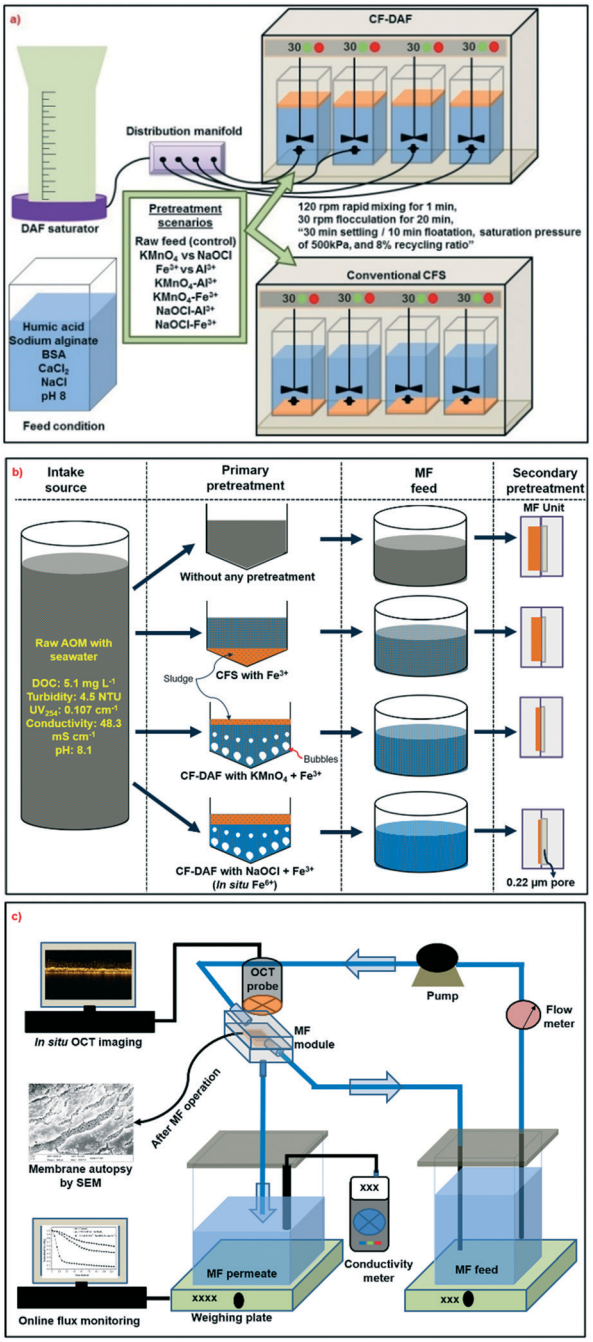

Fig. 1 Schematic diagram of the a) removal of AOM under CFS and CF-DAF methods, b) schematic diagram for different pretreatment strategies with successive microfiltration (MF, 0.22 μm membrane pore size) membrane unit for membrane fouling study, and c) membrane fouling comparison study for crossflow MF with CF-DAF pre-treated feed water samples using *in situ* and *ex situ* fouling characterization techniques.

Park Shatin, N.T., Hong Kong. The average quality of seawater used in this study can be found in the ESI† (Table S1); and (iii) an MF membrane fouling study with differently optimised pretreatment conditions.

For both the CFS and CF-DAF conditions, an oxidant was initially added to the feed solution, followed by the coagulant. In the case of CFS, rapid mixing was conducted at 120 rpm for 1 min (coagulation), slow mixing at 30 rpm for 20 min (flocculation), and settling for 30 min. The CF-DAF experiment was conducted following existing procedure,[48] which is 1 min of rapid mixing (120 rpm) during the coagulation stage, followed by 20 min of slow mixing (30 rpm) during flocculation, and 10 min of flotation by dissolved air at a saturation pressure of 500 kPa and 8% recycling ratio.[49–51] Samples were then taken from the sampling ports and filtered through 0.45 μm polyethersulphone (PES) filters prior to dissolved organic carbon (DOC) analysis and the ABTS test. All of the experiments were conducted in duplicate or triplicate. In the case of CF-DAF, the actual removal efficiency of individual parameters was calculated with a dilution factor ($1 + R/Q$), as presented in eqn (1).

$$\text{Removal efficiency}\ (\%) = \left(1 - \frac{C_f}{C_i}\right) \times \left(1 + \frac{R}{Q}\right) \times 100 \quad (1)$$

where, C_i and C_f are the initial and final concentrations, respectively; and R/Q is the recycle ratio (0–1).[51,52]

The MF experiments were conducted with a lab-scale membrane module set up at room temperature (25 ± 2 °C). Commercially available PES membranes (Membrane-Solutions, 0.22 μm pore size) were used in crossflow mode with an effective area of 24 cm^2 and at a constant pressure of 75 ± 1 kPa. Prior to each MF test, the membrane was thoroughly stabilised using DI water.

2.3. Analytical methods

Removal efficiencies for the synthetic AOM compounds were quantified in terms of DOC concentration and measured using a Shimadzu TOC-L analyser (precision ±2%, Shimadzu, Japan), according to the non-purgeable organic carbon measurement procedure.

The *in situ* generation of Fe^{6+} was detected by adding colourless ABTS to the solution containing Fe^{6+} to allow for characterization of green $ABTS^{\bullet+}$ radicals at 415 nm, as prescribed by a previous study.[53,54] The concentration of Fe^{6+} was measured using the indirect ABTS ultraviolet visible (UV-vis) method (UV-vis spectrophotometer, UV-2600, Shimadzu). As the absorbance of ABTS radicals at 415 nm is directly proportional to the concentration of Fe^{6+}, the concentration of aqueous Fe^{6+} was calculated by using eqn (2):

$$\text{Concentration of } Fe^{6+} = \frac{\Delta A_l^{415} \cdot V_{final}}{\varepsilon \cdot l \cdot V_{sample}} \quad (2)$$

where, ΔA_l^{415} is the absorbance at 415 nm after path length correction for the blank in cell of l, ε = molar extinction coefficient, l = path length of optical cell, V_{final} = final volume after addition of all reagents, and V_{sample} = volume of the original sample. Based on previous literature,[55–59] the molar extinction coefficient (ε) was considered to be 3.40 ± 0.05 × 10^4 M^{-1} cm^{-1}.

2.4. Membrane fouling factor and adsorption rate

Membrane fouling was assessed using the fouling factor (FF) parameter and computed by eqn (3):

$$FF = \left(1 - \frac{J}{J_0}\right) \times 100 \quad (3)$$

where, J/J_0 was the normalised flux during the 2 h filtration.

Development of fouling due to AOM concentration was quantified by the adsorption isotherm index (R_L),[60,61] as prescribed by eqn (4):

$$R_L = \frac{1}{1 + b \cdot \mathrm{AOM}_0} \quad (4)$$

where, b and AOM_0 are the Langmuir constant and initial AOM in terms of DOC concentration, respectively.

2.5. Surface morphology and fouling layer characterization

2.5.1. Scanning electron microscopy (SEM). Membrane fouling morphology was observed using SEM. The fouled membranes were gently cut from membrane modules, gold coated by sputtering for 80 s, and observed under SEM (ZEISS, Germany).

2.5.2. Monitoring of membrane fouling by optical coherence tomography (OCT). *In situ* monitoring of membrane fouling was performed using a spectral domain OCT (Ganymede II, Thorlabs GmbH, Dechau, Germany). An MF module with clear window was placed under the OCT probe to record the development of fouling over the course of the 2 h MF experiments. The 2D cross-sectional scans had a resolution of 800 × 1024 pixels, corresponding to 4.8 mm × 1.00 mm (width × depth). The OCT scans were processed with ImageJ software in order to regulate the contrast and brightness. The thicknesses of the fouling layers were calculated using a customised MATLAB code. Further detail can be found in the ESI† (S1).

3. Results and discussion

3.1. Optimization of oxidation and coagulation for AOM removal in CFS and CF-DAF

An in-depth study was conducted with a synthetic saline solution containing model AOM compounds, including HA (representing humic substances-like AOM), SA (representing HMW polysaccharides-like AOM), and BSA (representing HMW protein-like AOM) at pH 8 to mimic actual seawater conditions. In our previous study, a pH of 8 provided the optimal condition for the removal of AOM by oxidation-coagulation using a combination of NaOCl and Fe^{3+}.[54] Various combinations of the oxidant and coagulant in CFS and CF-DAF were then tested to find the optimal condition (Fig. 2).

3.1.1. Coagulation. As shown in Fig. 2a, the removal of AOM was not effective with Al^{3+} as the coagulant in conventional coagulation, with a coagulant dose of 3.0 mg L^{-1} only achieving an AOM removal of around 14% (remaining DOC 4.11 mg L^{-1}). In the case of CF-DAF, the maximum AOM removal achieved was up to 23% (remaining DOC 3.72 mg L^{-1}) with Al^{3+} dose of 3.0 mg L^{-1}. However, the overall AOM removal efficiency of the Fe^{3+} coagulant was relatively higher in both CFS and CF-DAF (Fig. 2b), which was 50% (remaining DOC 2.35 mg L^{-1}) and 59% (remaining DOC 1.89 mg L^{-1}) at a dose of 3.0 mg L^{-1}, respectively, compared to alum coagulation. This may be due to the more efficient sweep or adsorption mechanism of Fe^{3+} at seawater pH (pH 8) when compared to Al^{3+}.[62]

3.1.2. Coagulation with pre-oxidation. In the case of pre-oxidation using $KMnO_4$ as an oxidant, AOM removal by Al^{3+} coagulation improved to 55% (remaining DOC 2.09 mg L^{-1}) in CFS and to 64% (remaining DOC 1.70 mg L^{-1}) in CF-DAF at 3.0 mg L^{-1} of Al^{3+} with a dose of 1.5 mg L^{-1} $KMnO_4$ (Fig. 2c). Similarly, Fe^{3+} coagulation with $KMnO_4$ oxidation demonstrated a higher AOM removal than only coagulation (Fig. 2d).

In case of 1.5 mg L^{-1} $KMnO_4$ and 3.0 mg L^{-1} Fe^{3+} as oxidant–coagulant, AOM removal around 69% (remaining DOC 1.45 mg L^{-1}) was achieved with conventional CFS and 81% AOM removal (remaining DOC 0.84 mg L^{-1}) was achieved under the CF-DAF pretreatment scenario. As shown in eqn (5), the redox potential of $KMnO_4$ was 1.679 V at pH 8, that is near neutral or slightly alkaline condition.[30] Therefore, $KMnO_4$ can react with the dissolved organic matter, such as AOM, to generate MnO_2. After coagulation, MnO_2 accelerated the removal of AOM by adsorption and aggregation of tiny flocs. In addition, the combined application of $KMnO_4$–Al^{3+} pretreatment was shown to be more effective than only coagulation by Al^{3+}, as the saline AOM solution become slightly acidic (pH 7.33) upon oxidation, which further facilitated adsorption and charge neutralization during coagulation. While both Al^{3+} and Fe^{3+} coagulations are largely dependent on typical operating pH ranges, Fe^{3+} coagulant is relatively more efficient in a wider pH range than Al^{3+}.

$$MnO_4^- + 2H_2O + 3e^- \Rightarrow MnO_2 + 4OH^- \quad (5)$$

Similarly, dissolved AOM removal was enhanced in the case of NaOCl pre-oxidation with Al^{3+} as the coagulant (Fig. 2e). In CFS treatment, the lowest amount of DOC residue of 2.61 mg L^{-1} was achieved using 3.0 mg L^{-1} of Al^{3+} with 1.5 mg L^{-1} NaOCl. In CF-DAF with same dose of oxidant and coagulant (1.5 mg L^{-1}), the residual AOM was further minimised to 2.06 mg L^{-1} (56% removal). Compared to NaOCl–Al^{3+}, slightly higher AOM removal was achieved with $KMnO_4$–Al^{3+}, which was mainly due to the relatively strong redox potential of $KMnO_4$ compared to NaOCl (redox potential 1.482 V at pH 8).

However, the effect of pre-oxidation itself on AOM removal was marginal (Fig. 2g). Removal of AOM by 1.5 mg L^{-1} $KMnO_4$ was only 4% (remaining DOC 4.52 mg L^{-1}), whereas less than 1% removal (remaining DOC 4.65 mg L^{-1}) was recorded with 1.5 mg L^{-1} NaOCl. The formation of AOM-floc by oxidation-coagulation with $KMnO_4$ and Al^{3+} is due to strong adsorption of positively charged Al species onto

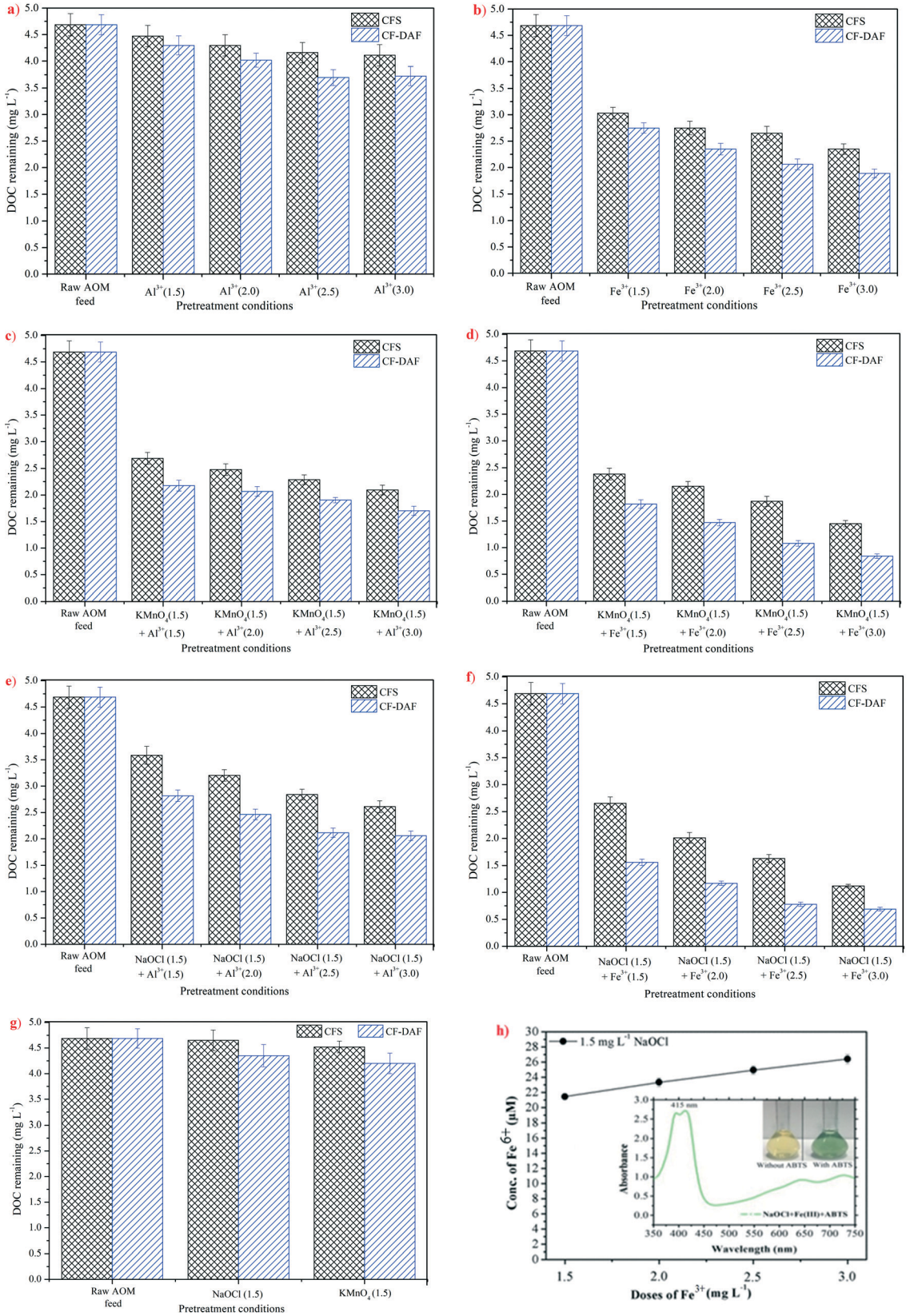

Fig. 2 Investigation of AOM removal during different CFS and *CF*-DAF scenarios of oxidant, coagulant comprise of NaOCl, $KMnO_4$, Al^{3+} and Fe^{3+} (a–g). The ABTS-UV_{vis} investigation to confirm *in situ* generation of Fe^{6+} (h).

negatively charged AOM fractions and the limited adsorption of MnO_2 precipitates. The formation of small compact structure flocs is attributed to charge neutralization as illustrated at ESI† Fig. S1(d). In CF-DAF, with the same dose of both oxidants, $KMnO_4$ and NaOCl, the AOM removal efficiency increased by 10% and 7%, respectively, compared to coagulation alone.

In the case of NaOCl–Fe^{3+} coagulation, a significant reduction in AOM was observed. Significant DOC removal was observed in CFS (65–76%) and CF-DAF (83–85%) with 1.5 mg L^{-1} of NaOCl and 2.5–3.0 mg L^{-1} doses of Fe^{3+}. The ligand exchange reaction between metal hydroxyl compounds and functional group of HA (*e.g.* hydroxyl and carboxylates),[63,64] may lead to adsorption of HA in the metallic solution of Fe and formation of humate complexes; furthermore, diffusivity and absorption of HA increased with an increase in NaCl concentration and decreasing pH levels and formation of Fe-biopolymer aggregates.[20,65,66] This indicates the ability of coagulation to destabilise dissolved AOM compounds by reducing their repulsive electrostatic forces. Following this reduction, strong attractive van der Waals forces lead to agglomeration.

Although floc formation during coagulation–flocculation is suggestive of charge neutralization mechanism, which plays a dominant role in the coagulation of AOM, our previous study[54] demonstrates that further generation of Fe^{6+} during wet chemical oxidation of Fe^{3+} and NaOCl may enhance the removal of AOM. The formation of Fe^{6+} was verified by the UV-ABTS method (Fig. 2h). The colourless ABTS solution reacted with Fe^{6+} to form greenish-blue $ABTS^{\bullet+}$ radicals, which were quantified by UV-vis method. Due to the higher molar absorptivity of $ABTS^{\bullet+}$ radicals compared to Fe^{6+}, more accurate and sensible results were obtained even with low concentrations of Fe^{6+}. Based on results and applying eqn (2), the *in situ* Fe^{6+} concentrations were detected as 1.31 mg L^{-1}.

3.2. AOM removal from real seawater

In the previous section, the removal efficiencies of synthetic saline-AOM water were investigated under different pretreatment conditions, in which CF-DAF with Fe^{3+} (2.5–3.0 mg L^{-1}) – NaOCl (1.5 mg L^{-1}) and Fe^{3+} (2.5–3.0 mg L^{-1}) – $KMnO_4$ (1.5 mg L^{-1}) were revealed as the optimised condition. Further, to investigate the performance of CF-DAF with actual seawater, the same AOM comprised of HA, SA and BSA were mixed with seawater while maintaining the initial DOC concentration at approximately 5.10 ± 0.23 mg C L^{-1}. The removal efficiency of real seawater-AOM was further investigated under different oxidant-coagulant doses of Fe^{3+}–NaOCl and Fe^{3+}–$KMnO_4$ to evaluate the best permeate quality for MF application. As illustrated in Fig. 3, AOM removal was relatively significant for peroxidation with NaOCl when compared to $KMnO_4$ with increases in Fe^{3+} doses. The maximum DOC removal of 74.7% was achieved for 2.5 mg L^{-1} Fe^{3+} with 1.5 mg L^{-1} NaOCl which was mainly attributed

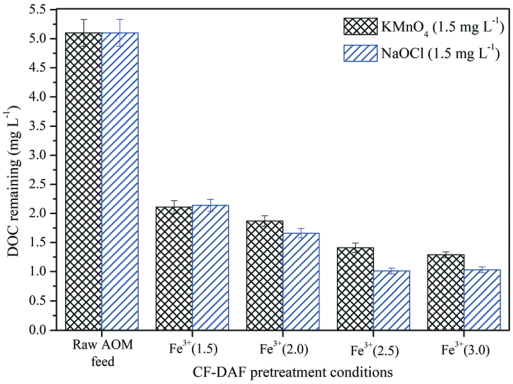

Fig. 3 CF-DAF pretreatment of real seawater-AOM with ferric coagulant with respective oxidant $KMnO_4$ and NaOCl.

to *in situ* Fe^{6+} generation during coagulation-flocculation process due to wet oxidation of Fe^{3+} and NaOCl.

3.3. Microfiltration

Membrane fouling potential for the MF membrane was evaluated with various feed solutions after coagulation and pre-oxidation in CF-DAF, and was compared with the scenario without pretreatment, as shown in Fig. 1b. Comparison was based on flux decline in MF operation, permeate quality, and fouling formation on the MF membrane. Qualities of MF feed and permeate water before and after the different pretreatments are given in Table 1.

3.3.1. Flux decline. Real seawater-AOM was treated by conventional CFS with Fe^{3+} and CF-DAF with $KMnO_4$–Fe^{3+} and NaOCl-Fe^{3+} (or *in situ* Fe^{6+}) respectively. Then, the treated seawater was adopted as the feed for MF to further monitor the fouling development and to eventually measure the fouling potential.

The patterns of flux decline in MF with differently pre-treated samples are presented in Fig. 4a. Rapid flux decline was recorded for untreated seawater-AOM. The lowest flux decline was observed in the application of CF-DAF with *in situ* Fe^{6+} produced by wet chemical oxidation with 2.5 mg L^{-1} dose of Fe^{3+} and 1.5 mg L^{-1} of NaOCl. Destabilization of particles played an important role in the effective removal of colloidal particles. Under aqueous conditions, the generated *in situ* Fe^{6+}, release oxygen (O_2) and $Fe(OH)_3$, which is the prime cause of instability for Fe^{6+}. The quantity of $Fe(OH)_3$ (floc) formation during the coagulation by *in situ* Fe^{6+} is relatively higher in comparison with coagulation by Fe^{3+} only. Hence, application of DAF can further remove AOM more effectively. This is because DAF has a relatively higher removal efficiency for low density, suspended organic matters (flocs) formed during coagulation, and adsorption of DOC on metal hydroxides generated from the Fe^{6+}.

The CF-DAF process with *in situ* Fe^{6+}, in which flocs and bubbles interacted to form stable floc-bubble aggregates, resulted in significantly less membrane fouling than CFS with only Fe^{3+}, in which fouling layers developed resulting in

Table 1 Water qualities of MF (0.22 μm pore, PES membrane) feed and permeate before and after different pretreatment scenarios

	Microfiltration feed						Microfiltration permeate				
Type of treatment scenario	pH	Turbidity (NTU)	Conductivity (mS cm^{-1})	DOC (mg L^{-1})	UV_{254} (cm^{-1})	Specific ultraviolet absorbance	Turbidity (NTU)	Conductivity (mS cm^{-1})	DOC (mg L^{-1})	UV_{254} (cm^{-1})	Specific ultraviolet absorbance
Seawater with AOM feed	8.1± 0.3	4.50 ± 0.21	48.3 ± 1.45	5.10 ± 0.23	0.107 ± 0.005	2.10	0.52 ± 0.02	41.2 ± 1.71	2.28 ± 0.11	0.035 ± 0.001	1.54
Coagulation–flocculation–sedimentation by 2.5 mg L^{-1} Fe^{3+}	7.7 ± 0.4	4.18 ± 0.11	36.5 ± 1.76	2.96 ± 0.09	0.061 ± 0.003	2.06	0.38 ± 0.01	33.8 ± 1.54	1.89 ± 0.09	0.025 ± 0.001	1.32
Coagulation–flocculation-DAF by 1.5 mg L^{-1} $KMnO_4$ + 2.5 mg L^{-1} Fe^{3+}	7.4± 0.2	2.12 ± 0.09	36.4 ± 1.75	1.41 ± 0.06	0.031 ± 0.001	2.20	0.26 ± 0.01	32.3 ± 1.37	1.21 ± 0.07	0.017 ± 0.001	1.40
Coagulation–flocculation-DAF by 1.5 mg L^{-1} NaOCl + 2.5 mg L^{-1} Fe^{3+}	7.5 ± 0.3	1.61 ± 0.06	35.9 ± 1.66	1.01 ± 0.05	0.019 ± 0.001	1.88	0.27 ± 0.01	31.1 ± 1.42	0.87 ± 0.04	0.010 ± 0.001	1.15

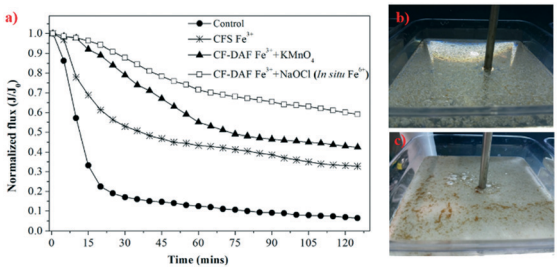

Fig. 4 a) Comparison of flux decline in MF operation for the removal of synthetic AOM in real seawater (initial DOC concentration was 5 mg-C per L) without any treatment (control), b) under CF-DAF by $KMnO_4$–Fe^{3+} pretreatment, and c) CF-DAF by *in situ* Fe^{6+}.

significant flux decline. In the case of CF-DAF with $KMnO_4$–Fe^{3+}, DOC removal after MF was 76% with a turbidity of 0.26 NTU. CF-DAF with *in situ* Fe^{6+} showed approximately 65% less flux decline at the end of filtration (Fig. 4a); moreover, DOC, turbidity, and UV_{254} of the MF permeate was reduced to 0.87 mg L^{-1} (83% removal), 0.27 NTU (94% removal), and 0.010 cm^{-1} (90% reduction), respectively. Additionally, *in situ* Fe^{6+} enhanced the production of flocs and subsequently increased the removal of AOM responsible for severe fouling (Fig. 4c), when compared to $KMnO_4$–Fe^{3+} (Fig. 4b).

3.3.2. Fouling observation using OCT and SEM. MF membrane fouling for different scenarios was investigated by *in situ* OCT and *ex situ* SEM technologies. OCT observation was conducted in transparent crossflow cells containing the MF membrane (0.22 μm PES membrane). Without any pretreatment of the seawater containing AOM model compounds, formation of a thick fouling layer was observed with a complete blockage of membrane pores, as shown in both the OCT image (Fig. 5a) and the SEM image (Fig. 6b). Due to the small size of HA, it can enter the membrane pores and is responsible for severe pore blockage with increasing filtration time; while both BSA and SA could form a stable

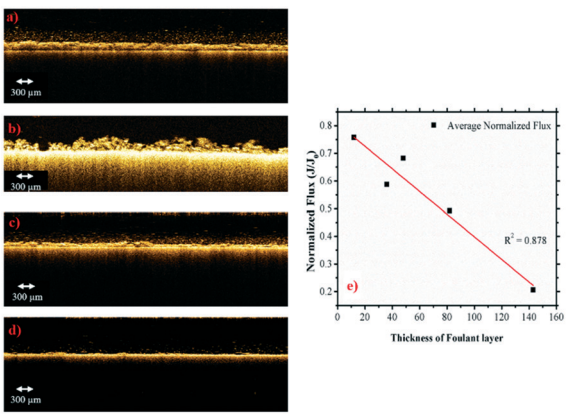

Fig. 5 OCT images of MF membranes with different pretreatments for the removal of synthetic AOM (initial DOC conc. approx. 5 mg C L^{-1}) in real seawater, a) without treatment (control), b) under CFS with Fe^{3+} scenario, c) under CF-DAF with KMnO4 and Fe^{3+} scenario, d) under CF-DAF with *in situ* Fe^{6+}, and e) the average normalised flux declines as a function of foulant thickness growth.

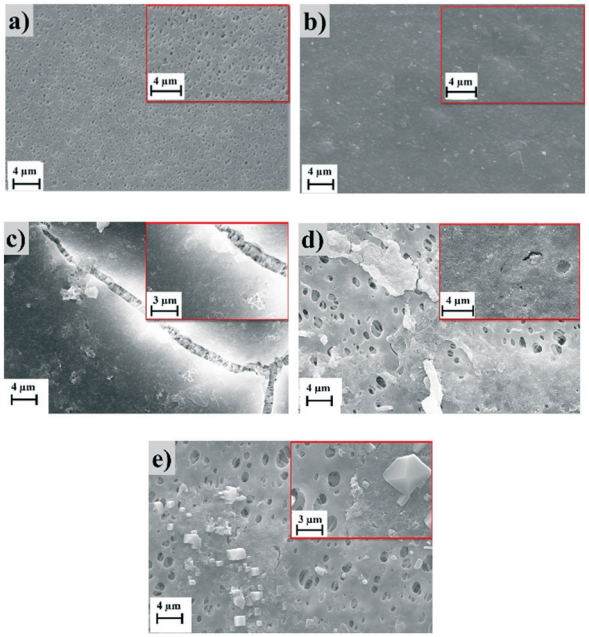

Fig. 6 SEM images (magnification 5k× and 15k×) of MF membranes with different pretreatments for the removal of synthetic AOM (initial DOC conc. approx. 5 mg C L^{-1}) in real seawater, a) virgin 0.22 μm pore PES membrane, b) without treatment (control), c) under CFS with Fe^{3+}, d) under CF-DAF with KMnO4 and Fe^{3+}, and e) under CF-DAF with *in situ* Fe^{6+}.

and sticky fouling layer along with other inorganic and colloidal particles, leading to a thick and irreversible fouling layer. These irreversible fouling layers were not removable with simple DI water flushing as shown in ESI† Fig. S2. With conventional CFS pretreatment using Fe^{3+}, the development of significant fouling layers was recorded during MF operation by *in situ* OCT scans (Fig. 5b) and after *ex situ* SEM image (Fig. 6c). After pretreatment with CF-DAF by $KMnO_4$–Fe^{3+}, a slightly thicker fouling layer was also observed (Fig. 5c and 6d). In the case of CF-DAF with *in situ* Fe^{6+} as pretreatment for MF, a negligible formation of fouling layer was observed by OCT (Fig. 5d) and by SEM (Fig. 6e).

A significant reduction in DOC by 1.01 mg L^{-1} (80%) and a reduction in turbidity to 1.61 NTU (64%) after CF-DAF with *in situ* Fe^{6+} mitigated fouling development during the MF operation. The average normalised flux decline with respect to fouling development (in terms of thickness) under different pretreatment scenarios, is shown in Fig. 5e. It can be concluded that the different pretreatment approaches led to various fouling behaviours on the membrane surface, thereby causing different flux decline patterns. Based upon the OCT and SEM observations, CF-DAF with *in situ* Fe^{6+} was selected as the optimal pretreatment scenario.

3.3.3. Fouling factor and AOM adsorption. Different initial AOM concentrations with respect to DOC were adopted to further understand the fouling mechanism during MF. AOM concentrations were tested in the range of 0.2–11.0 mg L^{-1} with a commercial PES (pore size 0.22 μm) membrane over the course of a 2 h MF experiment. Although the initial MF

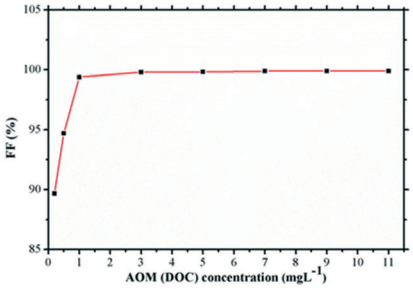

Fig. 7 Relationship between fouling factor (FF) and AOM (DOC) concentration.

filtration flux was nearly the same regardless of AOM concentration, a significant flux decline was recorded with an increase in AOM concentration and filtration time. Above 3.0 mg L^{-1} of AOM, a severe flux decline was observed during the initial 20–25 min of filtration time. The FF for the 2 h MF operation to remove AOM is presented in Fig. 7. The FF (%) increased rapidly with increases in the AOM concentration between 0.2 and 1.0 mg of DOC L^{-1}, and then stabilised above 3.0 mg L^{-1} of AOM due mainly to complete pore blocking and concentration polarization by AOM adsorption or fouling. The correlation between initial AOM fouling and FF was computed, and it was found that the Langmuir constant (b) and maximum FF (FF_{max}) were 38.68 and 99.89%, respectively. The R_L values ranged from 0.0500 to 0.0009 for the PES membrane, which was attributed to the favourable absorption of AOM on the MF membrane.

4. Conclusions

This study demonstrates a method for controlling organic fouling occurrence in membrane-based separation units by pretreatment of marine AOM. Pretreatment was comprised of pre-oxidation, coagulation, and DAF for the efficient removal of dissolved AOM. Different oxidant–coagulant combinations comprised of NaOCl, $KMnO_4$, Al^{3+} and Fe^{3+} were adopted for the pretreatment while synthetic AOM was prepared with HA, SA and BSA. The main conclusions of this study are as follows:

- Pre-oxidation–coagulation with NaOCl and Fe^{3+} was found to be relatively superior, demonstrating the highest AOM removal in terms of DOC and turbidity. Optimized DOC removal was achieved with 2.5–3.0 mg L^{-1} Fe^{3+} and 1.5 mg L^{-1} NaOCl due to the generation of 1.31 mg L^{-1} *in situ* Fe^{6+}, which was confirmed by ABTS-UV_{vis} method. Further by introducing DAF for 10 min flotation period with 8% recycling ratio at a saturation pressure of 500 kPa after oxidation–coagulation, the DOC and turbidity could be removed up to 80% and 64%, respectively.
- The pretreated AOM-seawater were further examined for fouling development in PES (0.22 μm) MF membranes. The pretreatment scenario, CF-DAF by 1.5 mg L^{-1} NaOCl and 2.5 mg L^{-1} Fe^{3+}, was observed for the least fouling development under *in situ* OCT monitoring compared to other pretreatment, or without pretreatment.

List of acronyms

ABTS	2,2-Azino-bis(3-ethylbenzothiazoline-6-sulphonic acid)
AOM	Algal organic matter
CFS	Coagulation–flocculation–sedimentation
CF-DAF	Coagulation–flocculation-dissolved air flotation
DAF	Dissolved air flotation
DOC	Dissolved organic carbon
HA	Humic acid
HS	Humic substances
NOM	Natural organic matter
OCT	Optical coherence tomography
SA	Sodium alginate

Conflicts of interest

There are no conflicts of interest to declare.

Acknowledgements

This research was financially supported by the Research Grants Council of Hong Kong for Early Career Scheme (Project number: 21201316) and General Research Fund (Project number: 11207717), and Basic Science Research Program through the National Research Foundation of Korea (NRF) funded by the Ministry of Education (2017R1A6A3A04004335).

References

1 A. Criscuoli and A. Figoli, *J. Hazard. Mater.*, 2019, **370**, 147–155.
2 D. Adeba, M. L. Kansal and S. Sen, *Sustain. Water Resour. Manag.*, 2015, **1**, 71–87.
3 G. R. Singh, M. K. Jain and V. Gupta, *Nat. Hazards*, 2019, **99**, 611–635.
4 N. Ekhtiari, A. Agarwal, N. Marwan and R. V. Donner, *Chaos*, 2019, **29**, 063116.
5 B. Yadav, S. Mathur, S. Ch and B. K. Yadav, *Hydrol. Sci. J.*, 2018, **63**, 210–226.
6 D. Kumar, D. S. Arya, A. R. Murumkar and M. M. Rahman, *Int. J. Climatol.*, 2014, **34**, 1395–1404.
7 N. K. Khanzada, S. J. Khan and P. A. Davies, *Desalination*, 2017, **406**, 44–50.
8 J. Guo, D. Y. S. Yan, F. L. Y. Lam, B. J. Deka, X. Lv, Y. H. Ng and A. K. An, *Chem. Eng. J.*, 2019, **378**, 122137.
9 N. K. Khanzada, M. U. Farid, J. A. Kharraz, J. Choi, C. Y. Tang, L. D. Nghiem, A. Jang and A. K. An, *J. Membr. Sci.*, 2019, 117672.
10 E. J. Lee, B. J. Deka, J. Guo, Y. C. Woo, H. K. Shon and A. K. An, *Environ. Sci. Technol.*, 2017, **51**, 10117–10126.
11 L. Chekli, E. Corjon, S. A. A. Tabatabai, G. Naidu, B. Tamburic, S. H. Park and H. K. Shon, *J. Environ. Manage.*, 2017, **201**, 28–36.
12 C. Dreszer, A. D. Wexler, S. Drusová, T. Overdijk, A. Zwijnenburg, H. C. Flemming, J. C. Kruithof and J. S. Vrouwenvelder, *Water Res.*, 2014, **67**, 243–254.
13 T. Nguyen, F. A. Roddick and L. Fan, *Membranes*, 2012, **2**, 804–840.
14 W. Yu, L. Xu, N. Graham and J. Qu, *Sci. Rep.*, 2014, **4**, 6513.
15 A. K. An, J. Guo, S. Jeong, E. J. Lee, S. A. A. Tabatabai and T. O. Leiknes, *Water Res.*, 2016, **103**, 362–371.
16 J. Guo, M. U. Farid, E. J. Lee, D. Y. S. Yan, S. Jeong and A. Kyoungjin An, *J. Membr. Sci.*, 2018, **551**, 12–19.
17 M. U. Farid, N. K. Khanzada and A. K. An, *Desalination*, 2019, **456**, 74–84.
18 X. Zhang, M. C. E. Devanadera, F. A. Roddick, L. Fan and M. L. P. Dalida, *Water Res.*, 2016, **103**, 391–400.
19 D. A. Ladner, D. R. Vardon and M. M. Clark, *J. Membr. Sci.*, 2010, **356**, 33–43.
20 S. A. Alizadeh Tabatabai, J. C. Schippers and M. D. Kennedy, *Water Res.*, 2014, **59**, 283–294.
21 Z. U. Rehman, S. Jeong, S. A. A. Tabatabai, A.-H. Emwas and T. Leiknes, *Desalin. Water Treat.*, 2017, **69**, 1–11.
22 B. J. Deka, E. J. Lee, J. Guo, J. Kharraz and A. K. An, *Environ. Sci. Technol.*, 2019, **53**(9), 4948–4958.
23 E. J. Lee, A. K. J. An, P. Hadi and D. Y. S. Yan, *Chem. Eng. J.*, 2016, **284**, 61–67.
24 N. Prihasto, Q. F. Liu and S. H. Kim, *Desalination*, 2009, **249**, 308–316.
25 S. Jeong, Y. J. Choi, T. V. Nguyen, S. Vigneswaran and T. M. Hwang, *J. Membr. Sci.*, 2012, **411–412**, 173–181.
26 X. Tang, H. Zheng, B. Gao, C. Zhao, B. Liu, W. Chen and J. Guo, *J. Hazard. Mater.*, 2017, **332**, 1–9.
27 L. Chekli, E. Corjon, S. A. A. Tabatabai, G. Naidu, B. Tamburic, S. H. Park and H. K. Shon, *J. Environ. Manage.*, 2017, **201**, 28–36.
28 L. O. Villacorte, Y. Ekowati, H. Winters, G. L. Amy, J. C. Schippers and D. Kennedy, *Desalin. Water Treat.*, 2013, **51**, 1021–1033.
29 P. Jia, Y. Zhou, X. Zhang, Y. Zhang and R. Dai, *Water Res.*, 2018, **131**, 122–130.
30 J. Jiang and B. Lloyd, *Water Res.*, 2002, **36**, 1397–1408.
31 A. Talaiekhozani, M. R. Talaei and S. Rezania, *J. Environ. Chem. Eng.*, 2017, **5**, 1828–1842.
32 D. Lv, L. Zheng, H. Zhang and Y. Deng, *Environ. Sci.: Water Res. Technol.*, 2018, **4**, 701–710.
33 M. A. Cataldo Hernández, A. May, A. Bonakdapour, M. Mohseni and D. P. Wilkinson, *Can. J. Chem.*, 2017, **95**, 105–112.
34 J.-Q. Jiang, *J. Chem. Technol. Biotechnol.*, 2014, **89**, 165–177.
35 J. Q. Jiang and B. Lloyd, *Water Res.*, 2002, **36**, 1397–1408.
36 A. Talaiekhozani, M. Salari, M. R. Talaei, M. Bagheri and Z. Eskandari, *J. Environ. Manage.*, 2016, **184**, 204–209.
37 B. J. Deka, S. Jeong, S. A. Alizadeh Tabatabai and A. K. An, *Chemosphere*, 2018, **206**, 718–726.
38 J. Diak and B. Örmeci, *J. Environ. Manage.*, 2018, **216**, 406–420.
39 A. Talaiekhozani, M. R. Talaei and S. Rezania, *Biochem. Pharmacol.*, 2017, **5**, 1828–1842.
40 A. K. Verma, R. R. Dash and P. Bhunia, *J. Environ. Manage.*, 2012, **93**, 154–168.

41 S. Chellam and M. A. Sari, *J. Hazard. Mater.*, 2016, **304**, 490–501.
42 W. Gan, V. K. Sharma, X. Zhang, L. Yang and X. Yang, *J. Hazard. Mater.*, 2015, **292**, 197–204.
43 X. Sun, Q. Zhang, H. Liang, L. Ying, M. Xiangxu and V. K. Sharma, *J. Hazard. Mater.*, 2016, **319**, 130–136.
44 D. Xia, C. He, L. Zhu, Y. Huang, H. Dong, M. Su, M. A. Asi and D. Bian, *J. Environ. Monit.*, 2011, **13**, 864–870.
45 S. Jeong, T. Leiknes, S. Lee, J.-G. Lee, L. Fortunato, Y. Jang and N. Ghaffour, *J. Membr. Sci.*, 2017, **546**, 50–60.
46 Y. Wang, L. Fortunato, S. Jeong and T. O. Leiknes, *Sep. Purif. Technol.*, 2017, **184**, 26–33.
47 C. Haisch and R. Niessner, *Water Res.*, 2007, **41**, 2467–2472.
48 J. K. Edzwald, *Water Sci. Technol.*, 1995, **31**, 1–23.
49 J. Haarhoff and J. K. Edzwald, *Desalination*, 2013, **311**, 90–94.
50 Y. Shutova, B. L. Karna, A. C. Hambly, B. Lau, R. K. Henderson and P. Le-Clech, *Desalination*, 2016, **383**, 12–21.
51 M. R. Teixeira and M. J. Rosa, *Sep. Purif. Technol.*, 2007, **53**, 126–134.
52 J. Guo, B. J. Deka, K.-J. Kim and A. K. An, *Desalination*, 2019, **468**, 114054.
53 M. Feng, X. Wang, J. Chen, R. Qu, Y. Sui, L. Cizmas, Z. Wang and V. K. Sharma, *Water Res.*, 2016, **103**, 48–57.
54 B. J. Deka, S. Jeong, S. A. Alizadeh Tabatabai and A. K. An, *Chemosphere*, 2018, **206**, 718–726.
55 D. Tiwari, *Ferrites and Ferrates: Chemistry and Applications in Sustainable Energy and Environmental Remediation*, ed. V. K. Sharma, R. Doong, H. Kim, R. S. Varma and D. D. Dionysiou, American Chemical Society, Washington DC, 2016, ch. 7, vol. 1238, pp. 161–220.
56 D. Tiwari, J. K. Yang and S. M. Lee, *Environ. Eng. Res.*, 2005, **10**(6), 269–282.
57 D. Tiwari and S. M. Lee, in *Waste Water-Treatment and Reutilization*, ed. F. S. G. Einschlag, InTech, Croatia, 2011, ch. 12, pp. 241–276.
58 Y. Lee, J. Yoon and U. Von Gunten, *Water Res.*, 2005, **39**, 1946–1953.
59 M. A. Cataldo Hernández, A. May, A. Bonakdapour, M. Mohseni and D. P. Wilkinson, *Can. J. Chem.*, 2017, **95**, 1332.
60 A. K. An, J. Guo, E. J. Lee, S. Jeong, Y. Zhao and T. Leiknes, *J. Membr. Sci.*, 2016, **525**, 57–67.
61 M. M. Rao, D. K. Ramana, K. Seshaiah, M. C. Wang and S. W. C. Chien, *J. Hazard. Mater.*, 2009, **166**, 1006–1013.
62 A. Adin, Y. Soffer and R. Ben Aim, *Water Sci. Technol.*, 1998, **38**, 27–34.
63 J. W. Guthrie, R. Mandal, M. S. A. Salam, N. M. Hassan, J. Murimboh, C. L. Chakrabarti, M. H. Back and D. C. Grégoire, *Anal. Chim. Acta*, 2003, **480**, 157–169.
64 Q. Wang, C. Zhu, X. Huang and G. Yang, *Environ. Pollut.*, 2019, **254**, 113110.
65 E. Illés and E. Tombácz, *J. Colloid Interface Sci.*, 2006, **295**, 115–123.
66 A. Ebrahimi, M. Hajian, H. Pourzamani and H. Esmaeili, *Int. J. Environ. Health Eng.*, 2012, **1**, 33.

